# ACCURATE MINIMAX DESIGN OF VARIABLE FRACTIONAL-DELAY FILTERS USING LINEARIZED OCTAGONAL CONSTRAINTS

*Tian-Bo Deng*

Department of Information Science
Faculty of Science, Toho University
Miyama 2-2-1, Funabashi, Chiba 274-8510, Japan
E-mail: deng@is.sci.toho-u.ac.jp

## ABSTRACT

This paper proposes a linear programming (LP)-based minimax design of even-order finite-impulse-response (FIR) variable fractional-delay (VFD) digital filters. The original minimax design is a non-linear optimization problem. To convert this non-linear problem into a linear one, we apply the rotation theorem to linearize the non-linear constraints as linear ones through constraining the complex-valued errors of variable frequency response (VFR) inside an octagon in the complex plane such that the resulting constraints are linear functions of the VFD filter coefficients. Hence, the minimax design can be done by using an LP technique. An example is given to illustrate that an even-order VFD filter can be designed more accurately than using the decoupling LP approach that solves a pair of LP sub-problems separately.

## 1. INTRODUCTION

Variable digital filters have instantly changeable magnitude responses [1]-[4] or/and fractional-delay (FD) responses [5, 6]. Without redesigning a new filter, users can tune the frequency response of a variable digital filter on-line. This paper focuses on variable fractional-delay (VFD) filters that have found various applications in sampling rate conversion, discrete-time signal interpolations etc. One can find the details on various FD filters in the survey paper [7]. The simplest variable fractional-delay (VFD) filter is the so-called Lagrange-type VFD filter [6], but its passband width is very narrow. To speed up the Lagrange-type VFD filtering, symmetric structures for both even-order and odd-order Lagrange-type VFD filters have been derived and proved [8, 9, 10]. To achieve wide-band VFD filtering, various methods have been developed [10]-[17]. Most of the methods are weighted-least-squares (WLS) designs that minimize the total error energy of variable frequency response (VFR).

This paper prsesents a new minimax method for designing even-order FIR VFD filters that minimizes the peak error (maximum absolute error) of the VFR. Since the VFR error is complex-valued, which includes both real-part and imaginary-part, the minimax design is inherently non-linear. To simplify this non-linear problem as a linear one such that it can be easily solved by utilizing a linear programming (LP) technique, we first convert the non-linear constraints into linear ones. By doing so, the non-linear minimax design can be linearized as an LP problem and can be solved easily. We will show that both the real-part error and imaginary-part error of the VFR error are mutually independent, so the two errors can be separately minimized, i.e., the non-linear minimax design can be decoupled into a pair of separate designs [19]. This decoupling approach is very simple and has low design complexity, but may cause a large deviation from the true minimax design. The worst-case deviation may be about 3 dB. The reason for this is that the complex-valued VFR errors are only constrained within a square in the complex plane and if both the real-part error and imaginary-part error reach the maximum, then the absolute VFR error will be $\sqrt{2}$ the real-part error (or imaginary-part error). To improve the design accuracy, this paper proposes a more accurate technique for linearizing the original non-linear constraints. The new minimax design methodology is to constrain the VFR errors within an octagon, which can be regarded as an application of the rotation theorem [20, 21]. Such approaches have been applied for designing constant FIR and IIR filters [22, 23]. Since an octagon is closer to a circle (true minimax design) than a square, the largest deviation can be reduced, which leads to a more accurate VFD filter. We will use an example to show that the octagonally constrained LP yields a more accurate VFD filter than the decoupling LP.

## 2. OCTAGONALLY CONSTRAINED LP DESIGN

In this section, we first briefly review the VFR and its error of an even-order VFD filter and show that the complex-valued VFR error can be separated into real part and imaginary part so that the decoupling LP design is possible [19]. Then, we linearize the non-linear constraints as linear ones through constraining the complex-valued VFR errors inside an octagon. As compared with the decoupling design, since the number of constraints increases, the computational complexity required in the octagonally constrained LP design also increases. This trades off the higher design accuracy.

The desired VFR of an even-order FIR VFD filter is

$$H_{\rm d}(\omega, p) = e^{-j\omega p} = \cos(\omega p) - j\sin(\omega p) \qquad (1)$$

where $\omega \in [0, \alpha\pi]$ is the normalized angular frequency, the parameter $\alpha$ specifies the passband edge frequency $\alpha\pi$ , $0 < \alpha < 1$, and $p$ is the VFD parameter, $p \in [-0.5, 0.5]$.

As in [19], we use the transfer function

$$H(z, p) = \sum_{n=-N}^{N} h_n(p) z^{-n} \qquad (2)$$

to approximate (1), where the variable coefficients $h_n(p)$ are the $M$th-degree polynomials in $p$ as

$$h_n(p) = \sum_{m=0}^{M} a(n, m) p^m. \qquad (3)$$

 

Substituting (3) into (2) yields

$$\begin{aligned} H(z,p) &= \sum_{n=-N}^{N}\sum_{m=0}^{M} a(n,m)z^{-n}p^{m} \\ &= \sum_{m=0}^{M_{\mathrm{e}}} F_m(z)p^{2m} + \sum_{m=1}^{M_{\mathrm{o}}} G_m(z)p^{2m-1} \end{aligned} \tag{4}$$

with

$$\begin{aligned} F_m(z) &= \sum_{n=-N}^{N} a(n,2m)z^{-n} \\ G_m(z) &= \sum_{n=-N}^{N} a(n,2m-1)z^{-n} \end{aligned} \tag{5}$$

$$M_{\mathrm{e}} = \left\lfloor \frac{M}{2} \right\rfloor, \quad M_{\mathrm{o}} = \left\lceil \frac{M}{2} \right\rceil \tag{6}$$

where $F_m(z)$ and $G_m(z)$ are called sub-filters in the Farrow structure [5], and $\lfloor\,\rfloor$, $\lceil\,\rceil$ are floor function and ceiling function, respectively. We have proved in [14] that the sub-filters $F_m(z)$ have even-symmetric coefficients

$$a(-n,2m) = a(n,2m)$$

and $G_m(z)$ have odd-symmetric (anti-symmetric) coefficients

$$a(-n,2m-1) = -a(n,2m-1).$$

Furthermore, for $m=0$, we have $a(n,m)=\delta(n)$, thus $F_0(z)=1$. By generalizing the same-order sub-filters $F_m(z)$ and $G_m(z)$ in (5) into different-order case, we get

$$\begin{aligned} F_m(z) &= \sum_{n=-N_{em}}^{N_{em}} a(n,2m)z^{-n} \\ G_m(z) &= \sum_{n=-N_{om}}^{N_{om}} a(n,2m-1)z^{-n} \end{aligned} \tag{7}$$

where the subscript "e" means that the sub-filters $F_m(z)$ have *even*-symmetric coefficients

$$a(-n,2m) = a(n,2m)$$

and "o" denotes that $G_m(z)$ have *odd*-symmetric coefficients

$$a(-n,2m-1) = -a(n,2m-1).$$

Fig. 1 shows the Farrow structure with $M=3$, i.e., $(M_{\mathrm{e}},M_{\mathrm{o}})=(1,2)$. Thus, the frequency responses of $F_m(z)$ and $G_m(z)$ are

$$\begin{aligned} F_m(\omega) &= \sum_{n=0}^{N_{em}} b_{em}(n)\cos(n\omega) = \mathbf{c}_m^T\mathbf{b}_{em} \\ G_m(\omega) &= (-j)\cdot\sum_{n=1}^{N_{om}} b_{om}(n)\sin(n\omega) = (-j)\cdot\mathbf{s}_m^T\mathbf{b}_{om} \end{aligned} \tag{8}$$

where

$$\begin{aligned} b_{em}(n) &= \begin{cases} a(n,2m) & n=0 \\ 2a(n,2m), & n=1,2,\cdots,N_{em} \end{cases} \\ b_{om}(n) &= 2a(n,2m-1), \quad n=1,2,\cdots,N_{om} \end{aligned}$$

and

$$\begin{aligned} \mathbf{c}_m^T &= [1 \quad \cos(\omega) \quad \cos(2\omega) \quad \cdots \quad \cos(N_{em}\omega)] \\ \mathbf{s}_m^T &= [\sin(\omega) \quad \sin(2\omega) \quad \cdots \quad \sin(N_{om}\omega)] \end{aligned}$$

$$\mathbf{b}_{em} = \begin{bmatrix} b_{em}(0) \\ b_{em}(1) \\ \vdots \\ b_{em}(N_{em}) \end{bmatrix}, \quad \mathbf{b}_{om} = \begin{bmatrix} b_{om}(1) \\ b_{om}(2) \\ \vdots \\ b_{om}(N_{om}) \end{bmatrix}.$$

Therefore, we have

$$\begin{aligned} F_m(\omega)p^{2m} &= \sum_{n=0}^{N_{em}} b_{em}(n)\cos(n\omega)\cdot p^{2m} \\ &= \mathbf{f}_m^T\mathbf{b}_{em} \\ G_m(\omega)p^{2m-1} &= (-j)\cdot\sum_{n=1}^{N_{om}} b_{om}(n)\sin(n\omega)\cdot p^{2m-1} \\ &= (-j)\cdot\mathbf{g}_m^T\mathbf{b}_{om} \end{aligned}$$

with

$$\mathbf{f}_m^T = \mathbf{c}_m^T p^{2m}, \quad \mathbf{g}_m^T = \mathbf{s}_m^T p^{2m-1}.$$

Hence, the VFR of $H(z,p)$ can be written as

$$\begin{aligned} H(\omega,p) &= 1 + \sum_{m=1}^{M_{\mathrm{e}}} \mathbf{f}_m^T\mathbf{b}_{em} - j\sum_{m=1}^{M_{\mathrm{o}}} \mathbf{g}_m^T\mathbf{b}_{om} \\ &= 1 + \mathbf{f}^T\mathbf{b}_{\mathrm{e}} - j\mathbf{g}^T\mathbf{b}_{\mathrm{o}} \\ &= \mathrm{Re}(\omega,p) - j\mathrm{Im}(\omega,p) \end{aligned} \tag{9}$$

where

$$\mathrm{Re}(\omega,p) = 1 + \mathbf{f}^T\mathbf{b}_{\mathrm{e}}, \quad \mathrm{Im}(\omega,p) = \mathbf{g}^T\mathbf{b}_{\mathrm{o}} \tag{10}$$

$$\begin{aligned} \mathbf{f}^T &= [\mathbf{f}_1^T \quad \mathbf{f}_2^T \quad \cdots \quad \mathbf{f}_{M_{\mathrm{e}}}^T] \\ \mathbf{g}^T &= [\mathbf{g}_1^T \quad \mathbf{g}_2^T \quad \cdots \quad \mathbf{g}_{M_{\mathrm{o}}}^T] \end{aligned}$$

and

$$\mathbf{b}_{\mathrm{e}} = \begin{bmatrix} \mathbf{b}_{\mathrm{e}1} \\ \mathbf{b}_{\mathrm{e}2} \\ \vdots \\ \mathbf{b}_{\mathrm{e}M_{\mathrm{e}}} \end{bmatrix}, \quad \mathbf{b}_{\mathrm{o}} = \begin{bmatrix} \mathbf{b}_{\mathrm{o}1} \\ \mathbf{b}_{\mathrm{o}2} \\ \vdots \\ \mathbf{b}_{\mathrm{e}M_{\mathrm{o}}} \end{bmatrix}. \tag{11}$$

The VFR error can be computed by using (1) and (9) as

$$\begin{aligned} e_{\mathrm{H}}(\omega,p) &= H(\omega,p) - H_{\mathrm{d}}(\omega,p) \\ &= e_{\mathrm{R}}(\omega,p) - je_{\mathrm{I}}(\omega,p) \end{aligned} \tag{12}$$

with

$$\begin{aligned} e_{\mathrm{R}}(\omega,p) &= \mathrm{Re}(\omega,p) - \cos(\omega p) \\ e_{\mathrm{I}}(\omega,p) &= \mathrm{Im}(\omega,p) - \sin(\omega p). \end{aligned} \tag{13}$$

Clearly, the real-part error $e_{\mathrm{R}}(\omega,p)$ is only the function of the coefficient vector $\mathbf{b}_{\mathrm{e}}$, and the imaginary-part error $e_{\mathrm{I}}(\omega,p)$ is only the function of $\mathbf{b}_{\mathrm{o}}$. Therefore, the coefficient vectors $\mathbf{b}_{\mathrm{e}}$ and $\mathbf{b}_{\mathrm{o}}$ can be separately minimized as

$$\begin{aligned} &\text{minimize} \quad \varepsilon_{\mathrm{R}} \\ &\text{subject to} \quad |e_{\mathrm{R}}(\omega,p)| \le \varepsilon_{\mathrm{R}} \end{aligned} \tag{14}$$

and

$$\begin{aligned} &\text{minimize} \quad \varepsilon_{\mathrm{I}} \\ &\text{subject to} \quad |e_{\mathrm{I}}(\omega,p)| \le \varepsilon_{\mathrm{I}}. \end{aligned} \tag{15}$$

This approach is called *decoupling LP design* [19], but it may cause a large deviation from the true minimax design. This is because both the real-part error $e_{\mathrm{R}}(\omega,p)$ and imaginary-part error $e_{\mathrm{I}}(\omega,p)$ are constrained within a square

$$\begin{aligned} |e_{\mathrm{R}}(\omega,p)| &\le \varepsilon \\ |e_{\mathrm{I}}(\omega,p)| &\le \varepsilon \end{aligned} \tag{16}$$

with $\varepsilon_{\mathrm{R}} = \varepsilon_{\mathrm{I}} = \varepsilon$. Thus, if both $|e_{\mathrm{R}}(\omega,p)|$ and $|e_{\mathrm{I}}(\omega,p)|$ take the maximum absolute value $\varepsilon$, then the maximum absolute VFR error is $\sqrt{2}\varepsilon$, i.e., the maximum deviation from the true minimax design is about 3 dB. As in the case of constant filter designs [22, 23], the rotation theorem can be applied to improve the design accuracy [20, 21]. Here, we constrain the VFR error $e_{\mathrm{H}}(\omega,p)$ such that both $e_{\mathrm{R}}(\omega,p)$ and $e_{\mathrm{I}}(\omega,p)$ are inside the octagon as shown in Fig. 2. That is, the maximum deviation from the true minimax design may be $(1-\cos(\pi/8))\varepsilon \approx 0.0761\varepsilon$. Consequently, the LP design can be formulated as

$$\begin{aligned} &\text{minimize} \quad \varepsilon \\ &\text{subject to} \quad |\Re\left[e_{\mathrm{H}}(\omega,p)e^{j\theta_k}\right]| \le \varepsilon\cos(\pi/8) \end{aligned} \tag{17}$$

with $\theta_k = k\pi/4$, $k = 0,1,2,3$, where $\Re[c]$ denotes the real-part of complex number $c$. Since

$$\begin{aligned} \Re\left[e_{\mathrm{H}}(\omega,p)e^{j\theta_k}\right] &= e_{\mathrm{R}}(\omega,p)\cos\theta_k + e_{\mathrm{I}}(\omega,p)\sin\theta_k \\ &= \left[1+\mathbf{f}^T\mathbf{b}_{\mathrm{e}} - \cos(\omega p)\right]\cos\theta_k \\ &\quad + \left[\mathbf{g}^T\mathbf{b}_{\mathrm{o}} - \sin(\omega p)\right]\sin\theta_k \end{aligned} \tag{18}$$

the constraint in (17) can be rewritten as

$$\begin{aligned} -\varepsilon\cos(\pi/8) + \Re\left[e_{\mathrm{H}}(\omega,p)e^{j\theta_k}\right] &\le 0 \\ -\varepsilon\cos(\pi/8) - \Re\left[e_{\mathrm{H}}(\omega,p)e^{j\theta_k}\right] &\le 0. \end{aligned} \tag{19}$$

Substituting (18) into (19) yields

$$\mathbf{A}_k\mathbf{x} \le \mathbf{d}_k, \quad k = 0,1,2,3. \tag{20}$$

with

$$\mathbf{A}_k = \begin{bmatrix} -\cos(\pi/8) & \mathbf{f}^T\cos\theta_k & \mathbf{g}^T\sin\theta_k \\ -\cos(\pi/8) & -\mathbf{f}^T\cos\theta_k & -\mathbf{g}^T\sin\theta_k \end{bmatrix}, \ \mathbf{x} = \begin{bmatrix} \varepsilon \\ \mathbf{b}_{\mathrm{e}} \\ \mathbf{b}_{\mathrm{o}} \end{bmatrix}$$

$$\mathbf{d}_k = \begin{bmatrix} [\cos(\omega p)-1]\cos\theta_k + \sin(\omega p)\theta_k \\ -[\cos(\omega p)-1]\cos\theta_k - \sin(\omega p)\theta_k \end{bmatrix}.$$

Combining (20) for $k = 0,1,2,3$ together arrives at

$$\mathbf{A} = \begin{bmatrix} \mathbf{A}_0 \\ \mathbf{A}_1 \\ \mathbf{A}_2 \\ \mathbf{A}_3 \end{bmatrix}, \ \mathbf{d} = \begin{bmatrix} \mathbf{d}_0 \\ \mathbf{d}_1 \\ \mathbf{d}_2 \\ \mathbf{d}_3 \end{bmatrix}.$$

Hence, the LP design (17) becomes

$$\begin{aligned} &\text{minimize} \quad \mathbf{c}^T\mathbf{x} \\ &\text{subject to} \quad \mathbf{A}\mathbf{x} \le \mathbf{d} \end{aligned} \tag{21}$$

with $\mathbf{c}^T = [1 \quad 0 \quad \cdots \quad 0]$. To perform the LP design, we first discretize the parameters $\omega$ and $p$, and then solve the LP problem (21) on a set of discrete points. Since both the ideal and actual frequency responses of the VFD filter (4) have conjugate symmetry with respect to $p = 0$, we only need to consider the half range $p \in [0, 0.5]$. Moreover, we can easily verify from (13) that

$$e_{\mathrm{R}}(\omega,p) = 0, \quad e_{\mathrm{I}}(\omega,p) = 0$$

for $p = 0$, i.e., the constraints in (19) are automatically met for $p = 0$. Thus, we need not impose any constraints on the LP design for $p = 0$. To solve (21), we discretize $\omega \in [0,\alpha\pi]$ and $p \in [0,0.5]$ with step sizes $\alpha\pi/(L_1-1)$ and $0.5/(L_2-1)$, respectively, and get grid points $(\omega_{l_1}, p_{l_2})$. Then, removing $p_{l_2} = 0$ leads to $L = L_1(L_2-1)$ discrete points. Since there are 8 constraints for each point as shown in (20), the total number of constraints is $8L = 8L_1(L_2-1)$.

## 3. DESIGN EXAMPLE

To approximate the ideal VFR in (1) with $\alpha = 0.9$, we set $(M_{\mathrm{e}}, M_{\mathrm{o}}) = (3,4)$ and the sub-filter orders

$$\begin{aligned} [N_{\mathrm{e}1} \quad N_{\mathrm{e}2} \quad N_{\mathrm{e}3}] &= [21 \quad 16 \quad 8] \\ [N_{\mathrm{o}1} \quad N_{\mathrm{o}2} \quad N_{\mathrm{o}3} \quad N_{\mathrm{o}4}] &= [36 \quad 29 \quad 19 \quad 7]. \end{aligned} \tag{22}$$

Thus, the total number of the VFD filter coefficients is 139.

To evaluate the design accuracy, we use the maximum VFR error (in dB) defined as

$$\varepsilon_{\mathrm{Max}} = \max\left\{20\log_{10}|e_{\mathrm{H}}(\omega,p)|, \omega \in [0,\alpha\pi], p \in [-0.5,0.5]\right\} \tag{23}$$

and the normalized root-mean-square (NRMS) VFR error

$$\varepsilon_2 = \left[\frac{\displaystyle\int_0^{\alpha\pi}\int_{-0.5}^{0.5}|e_{\mathrm{H}}(\omega,p)|^2 dp d\omega}{\displaystyle\int_0^{\alpha\pi}\int_{-0.5}^{0.5}|H_{\mathrm{d}}(\omega,p)|^2 dp d\omega}\right]^{1/2} \times 100\% \tag{24}$$

where $e_{\mathrm{H}}(\omega,p)$ is the VFR error in (12). Both the above two errors are numerically evaluated by discretizing $\omega \in [0,\alpha\pi]$ with step size $\alpha\pi/200$ and $p \in [-0.5,0.5]$ with step size $1/60$, which generates 201 points for $\omega \in [0,\alpha\pi]$ and 61 points for $p \in [-0.5,0.5]$. The design errors are

$$\begin{aligned} \varepsilon_{\mathrm{Max}} &= -101.2166\ (\mathrm{dB}) \\ \varepsilon_2 &= 0.000532\%. \end{aligned} \tag{25}$$

If the decoupling LP design is used, the resulting design errors are

$$\begin{aligned} \varepsilon_{\mathrm{Max}} &= -100.38\ (\mathrm{dB}) \\ \varepsilon_2 &= 0.000512\%. \end{aligned} \tag{26}$$

Therefore, the maximum error $\varepsilon_{\mathrm{Max}}$ is further reduced by applying the linearized octagonal constraints. This indicates

that constraining the complex-valued VFR errors within the octagon leads to more accurate minimax design than using a square approximation. As for the comparison with [17], since the decoupling LP design is better than the WLS design proposed in [17], it is obvious that the octagonally constrained LP is better than the WLS design [17].

Fig. 3 depicts the log magnitude VFR errors from the octagonally constrained LP design. Clearly, the design errors are considerably flat. To verify the flatness, Fig. 4 shows the log magnitude VFR errors $|e_{\rm H}(\omega,p)|$ for $p = 0.2$ , 0.35, 0.5, respectively. It is seen that the errors $|e_{\rm H}(\omega,p)|$ are almost equi-ripple. Fig. 5 depicts the VFD response and Fig. 6 plots its absolute errors whose maximum value is 0.001783.

## 4. CONCLUSION

This paper has presented an octagonally constrained LP approach for designing even-order FIR VFD filters. Instead of constraining the complex-valued VFR errors within the a square in the complex plane, we constrain the VFR errors inside an octagon. Since the octagon is closer to a circle (true minimax design) than a square, we can get more accurate minimax design than the decoupling LP design. A design example has been given to illustrate that the proposed octagonally constrained LP design has improved the design accuracy, i.e., the maximum VFR error can be further reduced. The octagonally constrained LP approach can also be extended to the odd-order VFD filter design.

## REFERENCES


[1] R. Zarour and M. M. Fahmy, "A design technique for variable digital filters," *IEEE Trans. Circuits Syst.*, vol. 36, no. 11, pp. 1473-1478, Nov. 1989.

[2] T.-B. Deng, "Design of recursive 1-D variable filters with guaranteed stability," *IEEE Trans. Circuits Syst. II, Analog Digit. Signal Process.*, vol. 44, no. 9, pp. 689-695, Sep. 1997.

[3] T.-B. Deng, "Weighted least-squares method for designing arbitrarily variable 1-D FIR digital filters," *Signal Process.*, vol. 80, no. 4, pp. 597-613, Apr. 2000.

[4] J.-J. Shyu, S.-C. Pei, and Y.-D. Huang, "Design of variable two-dimensional FIR digital filters by McClellan transformation," *IEEE Trans. Circuits Syst. I, Reg. Papers*, vol. 56, no. 3, pp. 574-582, Mar. 2009.

[5] C. W. Farrow, "A continuously variable digital delay element," *Proc. 1988 IEEE Int. Symp. Circuits Syst.*, vol. 3, pp. 2641-2645, Espoo, Finland, Jun. 6-9, 1988.

[6] G.-S. Liu and C.-W. Wei, "A new variable fractional sample delay filter with nonlinear interpolation," *IEEE Trans. Circuits Syst. II, Analog Digit. Signal Process.*, vol. 39, no. 2, pp. 123-126, Feb. 1992.

[7] T. I. Laakso, V. Valimaki, M. Karjalainen, and U. K. Laine, "Splitting the unit delay: Tools for fractional delay filter design", *IEEE Signal Processing Magazine*, vol. 13, no. 1, pp. 30-60, Jan. 1996.

[8] T.-B. Deng, "Coefficient-symmetries for implementing arbitrary-order Lagrange-type variable fractional-delay digital filters," *IEEE Trans. Signal Process.*, vol. 55, no. 8, pp. 4078-4090, Aug. 2007.

[9] T.-B. Deng, "Robust structure transformation for causal Lagrange-type variable fractional-delay filters," *IEEE Trans. Circuits Syst. I: Reg. Papers*, vol. 56, no. 8, pp. 1681-1688, Aug. 2009.

[10] T.-B. Deng, "Symmetric structures for odd-order maximally flat and weighted-least-squares variable fractional-delay filters," *IEEE Trans. Circuits Syst. I, Reg. Papers*, vol. 54, no. 12, pp. 2718-2732, Dec. 2007.

[11] T.-B. Deng, "Discretization-free design of variable fractional-delay FIR digital filters," *IEEE Trans. Circuits Syst. II, Analog Digit. Signal Process.*, vol. 48, no. 6, pp. 637-644, Jun. 2001.

[12] T.-B. Deng and W.-S. Lu, "Weighted least-squares method for designing variable fractional delay 2-D FIR digital filters," *IEEE Trans. Circuits Syst. II Analog Digit. Signal Process.*, vol. 47, pp. 114-124, Feb. 2000.

[13] T.-B. Deng, "Closed-form design and efficient implementation of variable digital filters with simultaneously tunable magnitude and fractional-delay," *IEEE Trans. Signal Process.*, vol. 52, no. 6, pp. 1668-1681, Jun. 2004.

[14] T.-B. Deng and Y. Lian, "Weighted-least-squares design of variable fractional-delay FIR filters using coefficient-symmetry," *IEEE Trans. Signal Process.*, vol. 54, no. 8, pp. 3023-3038, Aug. 2006.

[15] T.-B. Deng, "Hybrid structures for low-complexity variable fractional-delay FIR filters," *IEEE Trans. Circuits Syst. I, Reg. Papers*, vol. 57, no. 4, pp. 897-910, Apr. 2010.

[16] T.-B. Deng and Y. Nakagawa, "SVD-based design and new structures for variable fractional-delay digital filters," *IEEE Trans. Signal Process.*, vol. 52, no. 9, pp. 2513-2527, Sep. 2004.

[17] J.-C. Liu and S.-J. You, "Weighted least squares near-equiripple approximation of variable fractional delay FIR filters," *IET Signal Process.*, vol. 1, no. 2, pp. 66-72, Jun. 2007.

[18] C.-C. Tseng and S.-L. Lee, "Design of wideband fractional-delay filters using derivative sampling method," *IEEE Trans. Circuits Syst. I, Reg. Papers*, vol. 57, no. 8, pp. 2087-2098, Aug. 2010.

[19] T.-B. Deng, "Decoupling minimax design of low-complexity variable fractional-delay FIR digital filters," *IEEE Trans. Circuits Syst. I, Reg. Papers*, vol. 58, no. 11, Nov. 2011.

[20] K. Glashoff and K. Roleff, "A new method for Chebyshev approximation of complex-valued functions," *Math. Comput.* vol. 36, no. 153, pp.233-239, 1981.

[21] R. L. Streit and A. H. Nuttall, "A note on the semi-infinite programming approach to complex approximation," *Math. Comput.*, vol. 40, no. 162, pp. 599-605, 1983.

[22] X.-K. Chen and T. W. Parks, "Design of FIR filters in the complex domain," *IEEE Trans. Acoust. Speech, Signal Process.*, vol. 35, no. 2, pp. 144-153, Feb. 1987.

[23] C.-C. Tseng and S.-L. Lee, "Minimax design of stable IIR digital filter with prescribed magnitude and phase responses," *IEEE Trans. Circuits Syst. I, Fundam. Theory Appl.*, vol. 49, no. 4, pp. 547-551, Apr. 2002.

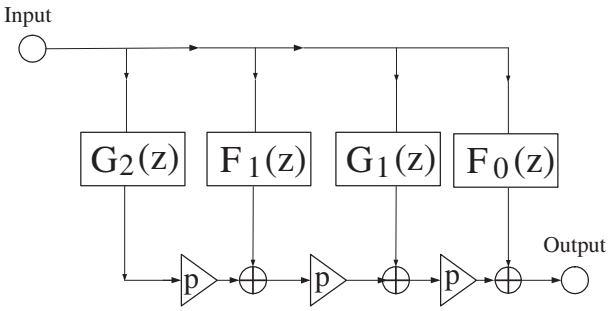


Fig. 1. Farrow structure with $(M_e, M_o) = (1,2)$.

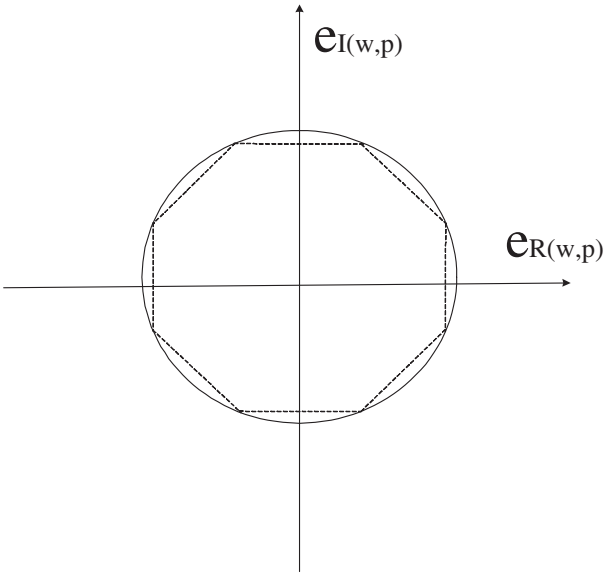


Fig. 2. Octagonally constrained VFR errors.

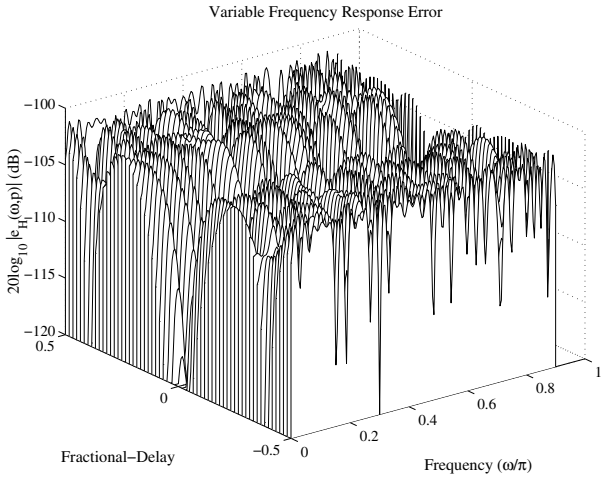


Fig. 3. Log magnitude VFR errors.

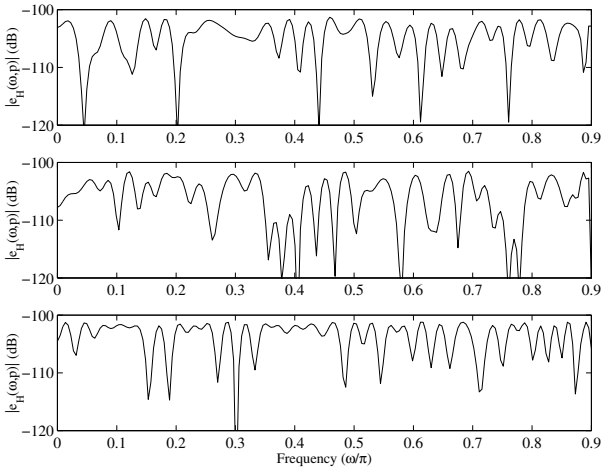


Fig. 4. Log magnitude VFR errors for $p = 0.2, 0.35, 0.5$.

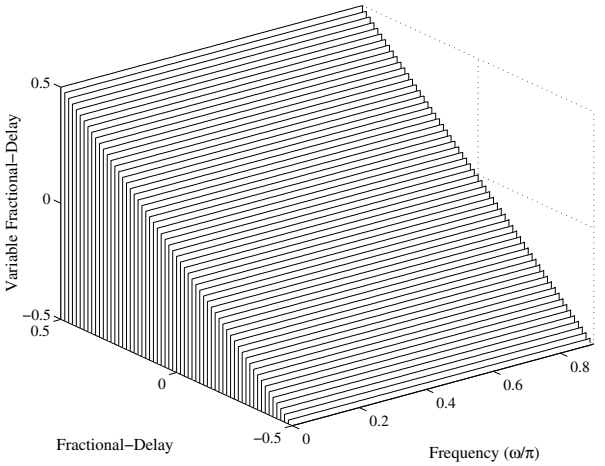


Fig. 5. VFD response.

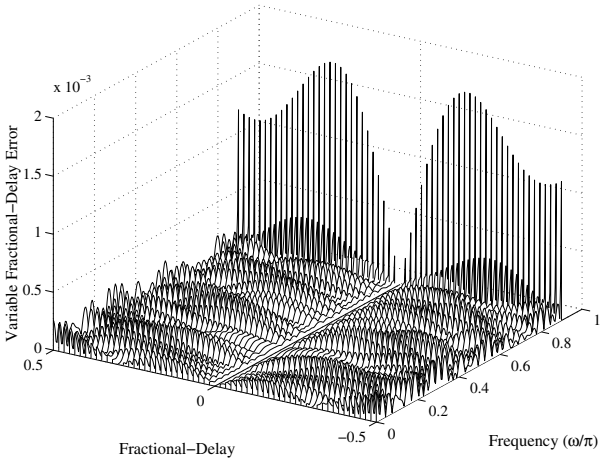


Fig. 6. Absolute VFD errors.